Soil surface change data of high spatio-temporal resolution from the plot to the catchment scale

Lea Epple[1], Oliver Grothum[1], Anne Bienert[1], and Anette Eltner[1]

[1]Institute of Photogrammetry and Remote Sensing, Dresden University of Technology, Helmholtzstr. 10, 01069 Dresden, Germany

Correspondence to: Lea Epple (lea.epple@tu-dresden.de), Anette Eltner (anette.eltner@tu-dresden.de)

Abstract

~~Limitations of current~~Although process-based soil erosion models are~~,~~ valuable tools for predicting and managing soil erosion, ~~lie particularly with today's~~ their limitations arise from constraints in integrating novel data possibilities~~availability~~, uncertainties in parameterisation~~ uncertainty~~, and the difficulties in integrating~~on~~ different process scales and their transitions~~ of changing environmental conditions~~. This study presents a ~~novel~~ unpresented approach to enhance soil erosion modelling through the utilisation of nested high-resolution spatio-temporal data obtained through structure from motion (SfM) photogrammetry. This technique permits comprehensive observation of soil surface elevation changes during precipitation events, encompassing data acquisition at diverse scales, from plot to slope to micro-catchment. The study presents a ~~worldwide~~ unique dataset that integrates high-resolution time-lapse photogrammetry, field measurements, and UAV (uncrewed aerial vehicle) photogrammetric data, collected over nearly four years. This dataset is intended to enhance the understanding of soil erosion processes and serve as a valuable resource for model evaluation and calibration. The authors encourage the broader scientific community to utilise and expand this dataset, which is expected to contribute to the development of more accurate soil erosion models, thereby improving predictions and management strategies.

1 Introduction

Soil erosion models constitute a valuable resource for stakeholders, policymakers and scientists in the context of soil erosion prediction and decision-making (Batista et al., 2019). From the extensive array of existing models, a variety of models have been developed for diverse scales and for particular process mapping inherent to the scale (Jetten & Favis-Mortlock, 2006). The evaluation of soil erosion models is a complex process, often constrained by the limitations of data availability and the inherent uncertainties in measuring erosion and generating model parameters (Batista et al., 2019; Pandey et al., 2016). The models frequently assume that the input parameters are stationary and that the data pertaining to the surface and soil are unchanging (Jetten & Favis-Mortlock, 2006). Consequently, they encounter difficulties in integrating updated observations that necessitate the consideration of changing model parameters. Furthermore, limitations are evident with regard to cross-scale process understanding and modelling, as well as with respect to the modelled resolution (Epple et al. 2022). A multitude of process-based soil erosion models have been developed for utilisation at field and catchment scales. The smallest of these models use~~are modelled at a~~ a resolution of 1 m (see, for example, Naranjo et al., 2021), thereby focusing on the dominant processes at these scales (Epple et al., 2022). To guarantee the dependability of the data generated by these models, it is essential to conduct continuous testing and model improvement at all scales (Batista et al., 2019).

The application of photogrammetric methodologies provides a novel opportunity for the evaluation and calibration of process-based soil erosion models. Structure from motion (SfM) photogrammetry, a method for camera-based surface measurements, has previously been employed for comprehensive monitoring of soil surface alterations during an artificial rainfall simulation and a natural thunderstorm event (Eltner et al., 2017). It has been demonstrated that this method is capable of detecting intra-experimental changes in soil surface topography at the micro-scale, due to the near-automatic processing involved (Eltner & Sofia, 2020). The potential for acquiring high-resolution digital elevation models (DEM) at high temporal frequency is made possible by time-lapse photogrammetry, as demonstrated by Jiang et al. (2020) for an artificial slope of 10 m length utilising a DEM acquisition frequency of five minutes. In the field of natural hazards, time-lapse photogrammetry has been employed to achieve cm-accurate estimation of rockfalls at few hourly intervals (Blanch et al., 2024~~1~~). Observations for soil erosion measurement so far mostly concentrate on single artificial rainfall events, with studies employing rainfall simulations in the laboratory (data acquisition frequency every 30 minutes, Yang et al., 2021) or in the field (data acquisition before and after the event, Ehrhardt et al., 2022) and do not take higher frequencies into account. ~~The former employed a frequency of 30 minutes, while the latter conducted observations before and after the event. The majority of~~

~~studies have concentrated on splash and interrill erosion (Hänsel et al., 2016), while others have considered seasonal changes (Wang et al., 2024), using an uncrewed aerial vehicle (UAV) to capture multiple datasets via SfM (Eltner et al., 2015). The potential for acquiring high-resolution digital elevation models (DEM) at high temporal frequency is made possible by time-lapse photogrammetry, as demonstrated by Jiang et al. (2020) for an artificial slope of 10 m length utilising a DEM frequency of five minutes. In the field of natural hazards, time-lapse photogrammetry has been employed to achieve cm-accurate estimation of rockfalls at few hourly intervals (Blanch et al., 2021).~~

~~An examination of the~~Moving from plot to catchment scale different soil erosion processes are prone to each scale and therefor ~~reveals that~~ a range of soil surface change processes are at work, exerting influence over different temporal intervals and spatial scales. These processes result in a continuous transformation of the soil surface. In order to achieve ~~a high level of resolution and~~ a comprehensive understanding of processes across different scales, we present a new and integrated nested cross-scale data set. This comprises time-lapse photogrammetric plot data, recorded at 10-60 second intervals during artificial rainfall simulations, field data captured on a daily basis~~ and~~, at 0.2 mm intervals during natural rainfall events and via UAV before and after tillage, and UAV data acquired at the micro-catchment scale. The field data were collected over a period of nearly four years. In a recent study, Eltner et al. (2025) demonstrate the value of such data by evaluating the RillGrow (Favis-Mortlock 2025) soil erosion model with high-resolution observations of rill evolution. Their findings highlight the ongoing challenge of equifinality for process-based soil erosion models and emphasise the need for further model development and data assimilation. They also underscore the potential of spatio-temporal high-resolution data for advancing this field of research. Based on high-resolution DEMs captured at 20-seconds intervals, Epple et al. (2025) observed soil settling and compaction processes at the onset of rainfall simulations. This provides an empirical approach for differentiating between these processes and erosional processes, thereby enhancing the applicability of photogrammetric data for soil erosion monitoring. It is our intention to make our data available to the soil erosion modelling community for the purposes of evaluation and calibration, as well as further development of soil erosion models, regarding, e.g., cross scale process ~~mapping~~prediction.

The following section presents the data acquisition structured by the three different scales using SfM photogrammetry. Subsequently, the data were subjected to a preliminary processing stage. The raw data, along with the processed data, are accessible in an open-source format, structured in accordance with the specifications outlined in Section 4.

2 Data acquisition

The data were acquired at three different scales (Tab. 1): by UAV-image capture on catchment scale~~plot scale via SfM during rainfall simulation~~, single slope scale by event-triggered monitoring posts and on the plot scale via SfM during rainfall simulation ~~by UAV-image capture on catchment scale~~.

Table 1: Summary of the observation scales, their time/duration of monitoring, their temporal resolution and size

scale	**catchment~~plot~~**	**slope**	**~~catchment~~plot**
time	~~up to 3 hours~~ single flights	3.5 years	~~single flights~~up to 3 hours
temporal resolution	~~10-20 s~~~~9 flights~~ yearly	~~D~~daily, ~~/~~ every 0.2 mm rainfall, before and after tillage	~~9 flights~~10-20 s
size (length x width)	~~3 x 1 m~~5.29 ha	60 x 12 m	~~5.29 ha~~3 x 1 m

Subsequently, the photogrammetric data underwent further processing, resulting in the generation of dense three-dimensional point clouds, which were converted to ~~(~~digital elevation models (DEMs), point precision maps and M3C2 (multiscale model to model cloud comparison) distance measures.

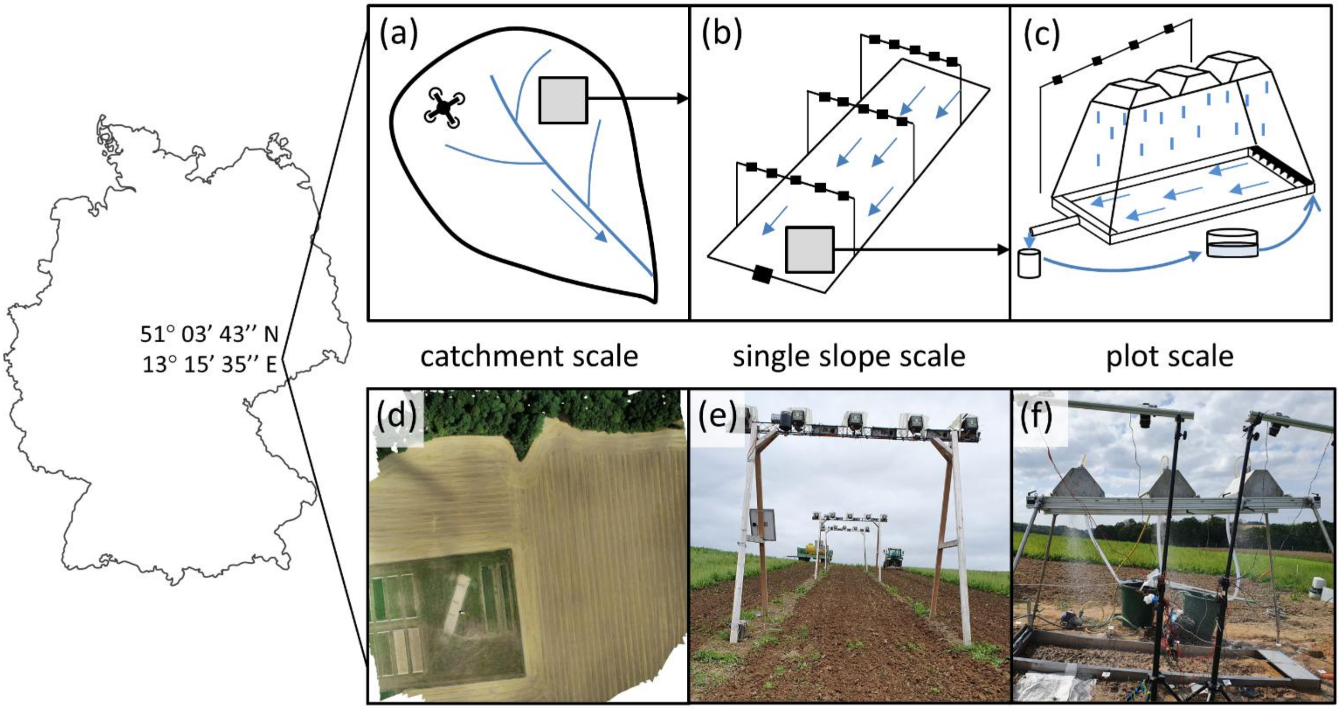

Figure 1: Location of the nested experimental setup in Saxony, Germany (map on the left). The upper row presents a schematic display, while the lower row shows images of the actual setup. The figures illustrated are the catchment scale (a, d), where SfM (structure from motion) is recorded by UAV (uncrewed aerial vehicle; d = UAV-orthophoto); the single slope scale (b, e) with a synchronised, rain-triggered camera setup on three monitoring stations~~posts~~; and the plot scale (c, f), nested within the slope scale using artificial rainfall simulations observed with time-lapse SfM (c is adapted from Schindewolf, 2012).

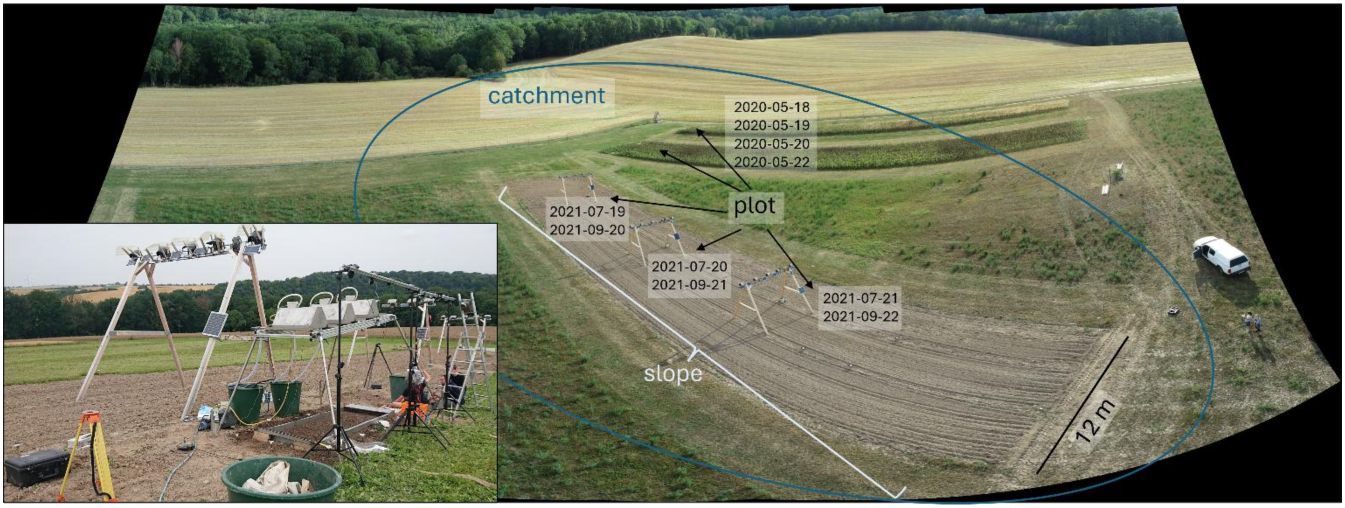

Figure 2: Image of the nested experimental setup with locations and dates of the ~~of the~~ artificial rainfall simulations. Image in the lower left corner shows the positioning of the rainfall simulation next to the middle monitoring post on the slope setup.

The nested data acquisition setup was situated in the hilly loess landscape in the vicinity of Nossen in the east of Germany (Fig. 1). The micro-catchment area, which is predominantly utilised for agricultural purposes and covers an area of 5.29 ha, drains to the north into the *Freiberger Mulde* (see Fig. 1d). The single slope, i.e., field, which is nested in the catchment area, is oriented north-northeast (51°03′43″ N, 13°15′35″ E) and exhibits a gradient of up to 15%. At the most detailed scale, the plot scale, synthetic rainfall simulations were carried out on 3 m² plots (Fig. 1c, f) situated on the single slope (Fig. 1b, e). The locations of the nested setup are ~~again~~ visualised in Fig. 2. Further rainfall simulations were conducted at multiple locations in the east of Germany, across a range of slopes, soil types, soil management practices, soil covers and soil bulk densities (blue flags in Fig. 3). The time frame, as well as soil and surface conditions for the data acquisition process is illustrated in Fig. 3 and can be found in more detail within the published data set.

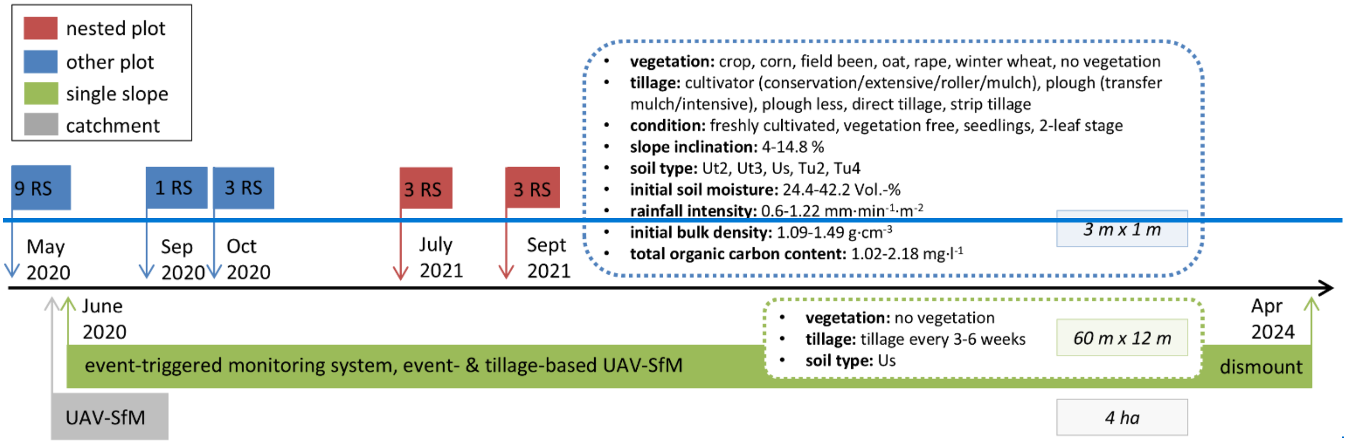

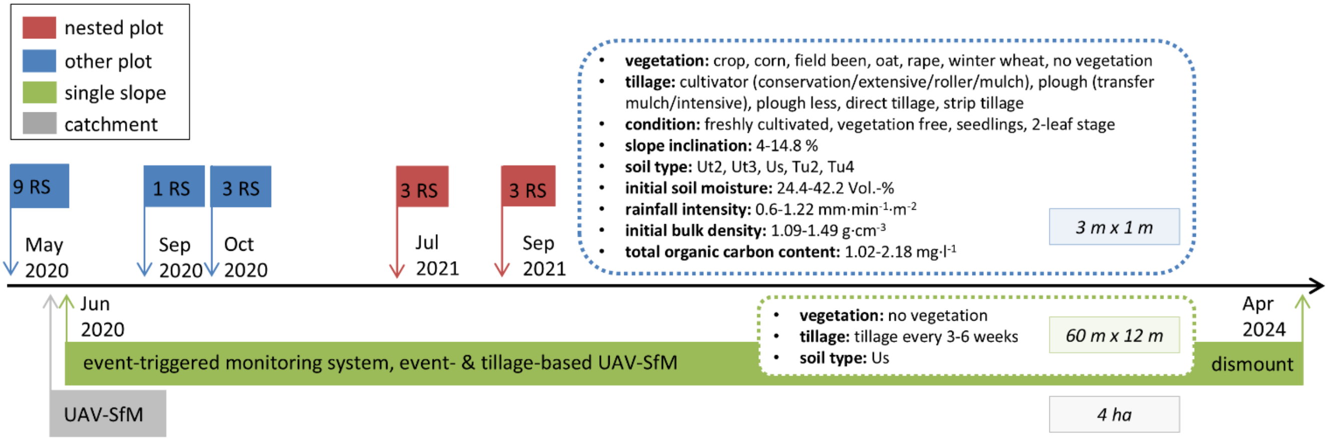

Figure 3: Timeline of the data collection over almost four years. The nested setup includes the catchment area (depicted in grey), the single slope (shown in green) and the plot with six rainfall simulations (RS) (illustrated in red). The remaining 13 RS (blue boxes) were carried out at different sites. The soil, rain and agricultural conditions, sampled and observed in the field and in the laboratory, are summarised in the dashed boxes. The magnitude of the observed scales is highlighted in each row. The following abbreviations are used: UAV = uncrewed aerial vehicle, SfM = structure from motion.

2.1Catchment scale

At the catchment scale, an orthophoto and a DEM were calculated via UAV-photogrammetry for the 2020-07-22 (Fig. 1d). The image data was acquired using a *DJI Phantom 4 RTK* UAV. Further ~~raw~~ image data ~~(*.raw format)~~ of the catchment ~~data were~~ was taken on nine days between April 2020 and September 2022, these are available in unprocessed form. The observation height was generally set to a range of 30-50 m, with nadir images resulting in a ground sampling distance of 2 cm. The data thus provides the basis for testing soil erosion models at the catchment scale and enabling modeller the upscaling ~~from~~ of~~the~~ slope scale parametrisation to the catchment scale. Therefore, the objective is not to calibrate ~~or evaluate~~ a model, but rather to serve as a high-resolution model input and for model testing.

2.2 Single slope scale

The single slope (see Tab. -1 for dimensions and Grothum et al. 2025 for more detail)~~, measuring 60 m in length and 12 m in width,~~ was situated within the catchment area and maintained in a clear state, with vegetation removed by means of ~~grubbing~~ cultivating downslope at a depth of 10 cm at three-to-six-week intervals. It was monitored over a period of almost 3.5 years (July~~y~~ 2020 to April 2024) by a total of 15 cameras mounted on three monitoring ~~posts~~stations. Five event-triggered and synchronised RGB cameras were installed on each monitoring ~~post~~ device, fixed on a traverse in 4 -m height ~~(resulting in a total of 15 cameras monitoring the entire slope~~), along with an Arduino-based control station connected to a rain gauge, taking pictures every 0.2 mm of rainfall (controlled by a tipping bucket). Furthermore, ~~T~~the cameras ~~on each post w~~were triggered at 10 a.m. daily (controlled by an RTC – real time clock)~~ and in response to 0.2 mm of rainfall (controlled by the tipping bucket of the rain gauge)~~. The areas observed by the monitoring ~~posts~~stations, which were 4 m wide and 7.5 m long (marked in yellow in Fig. 4a, d), were situated within the central portion of the field, which was ~~grubbered~~ cultivated in three parallel lines along the slope. The area was delineated by ground control points (GCPs) on the left and right sides~~ (Fig. 4)~~. The number of individual cameras and their positions are illustrated in Fig. 4a up until July 2022 and modified for the period after July 2022 in Fig. 4d. The modification, initiated due to storm damage, involved the rotation of two monitoring posts and their repositioning to face downwards, thereby facilitating the capture of ~~of~~ the bottom of the slope ~~bottom~~ more~~with greater~~ effectively~~icacy~~ and reducing the amount of rain droplets blown onto the camera lenses. A comprehensive~~n in-depth~~ description of this structure can be found by Grothum et al. (2025). In addition to the spatio-temporal high-resolution, event-triggered data acquisition at three positions (upper, middle, and lower slope) (Fig. 4), UAV-SfM data were collected over the entire slope before and after both rainfall events and tillage.

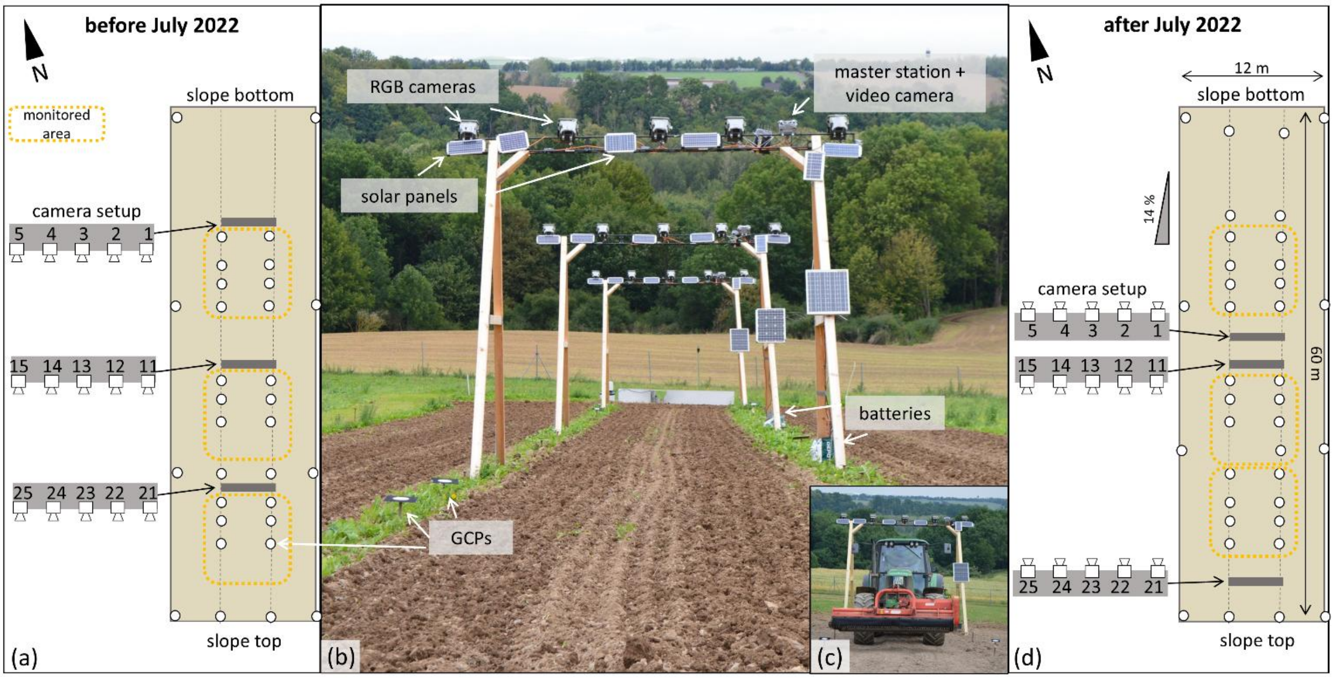

Figure 4: Monitoring setup on the slope scale with three monitoring ~~posts~~stations, each equipped with five RGB cameras (b). The schematic representation in (a) and (d) includes the camera designations and positions of the GCPs (ground control points). Figure (a) presents the setup employed until July 2022. Subsequently a slight modification was implemented as shown in Figure (d). The height of the posts was chosen to facilitate the mechanical removal of vegetation (c) while minimising potential restrictions.

2.3 Plot scale

~~Regarding the nested setup,~~ S~~s~~ix rainfall simulations were performed at the plot scale; encompassing the lower, middle and upper regions of the monitored slope in July and September 2021 (Fig. 3). Furthermore, a total of 13 additional rainfall simulations were carried out at various sites in Saxony and Thuringia and under different conditions between May and October 2020 (Fig. 3). More information on each individual plot can be found in an overview table as part of the data publication this~~e~~ article accompanies. GCPs were installed around each plot, driven at least 10 cm into the ground, in order to enable georeferencing and ensure stability during the experiment. The rainfall simulator used is described in detail in Schindewolf ~~&~~and Schmidt (2012). The precipitation is dispersed onto the ground from three rain hoods with oscillating nozzles at an elevation of 2 m. The velocity, distribution and size of the raindrops produced by the *VeeJet 80/100* nozzles are comparable to those of a heavy rainfall event (Kainz et al., 1992). At the base of the plot, which was enclosed by metal sheets and had a length of 3 m and a width of 1 m, a sediment collector was used to facilitate the collection and measurement of runoff and sediment concentration (see also Tab. 3). At the outset of the rainfall simulation, the intensity of the precipitation was gauged by enclosing the plot with a protective sheet and measuring the total discharge. Thereafter, the infiltration experiment started (Fig. 5, A in timeline). Once a steady state of infiltration had been reached, the apparatus designed to simulate slope lengths exceeding 3 m was activated. The runoff experiment (Fig. 5, B in~~,~~ timeline) was conducted for a further 10 to 14 minutes. Subsequently, the water supply feeding~~s~~ surface runoff and rainfall was terminated for approximately one hour, after which the repetition was carried out. An individual camera setup on posts at heights of 1.5 to 3 m, comprising eight to eleven synchronised digital single-lens reflex (SLR) cameras (schematic in Fig. 5), captured images to generate DEMs at 10-, 20- and 60-second intervals (A – runoff experiment, B – infiltration experiment, and break, ~~compare~~ referring to the camera symbols~~s~~ in the timeline in Fig. 5). ~~An e~~Exceptions are t~~T~~he rainfall simulations carried out ~~during~~ in September and October 2020. These were performed with a minor alteration, ~~omitting~~ the first ~~runoff~~ infiltration experiment ~~and transitioning~~was directly followed by~~to the~~ a break before the second ~~following the~~ infiltration experiment took place, followed by a- runoff experiment (corresponding to Fig. 5, the timeline for these simulations can be described as A-break-A-B). As an~~In~~ addition to the camera monitoring system, a camera was utilised for all-round SfM data capture during the break and before and after the experiment. This was done in order to estimate 3D models with images acquired from the most suitable perspectives, with the aim of avoiding data gaps due to occlusions as much as possible. This offers a different perspective and point density ~~than the~~compared to the synchronised camera setup resulting in a valuable data s~~-~~et for model input.

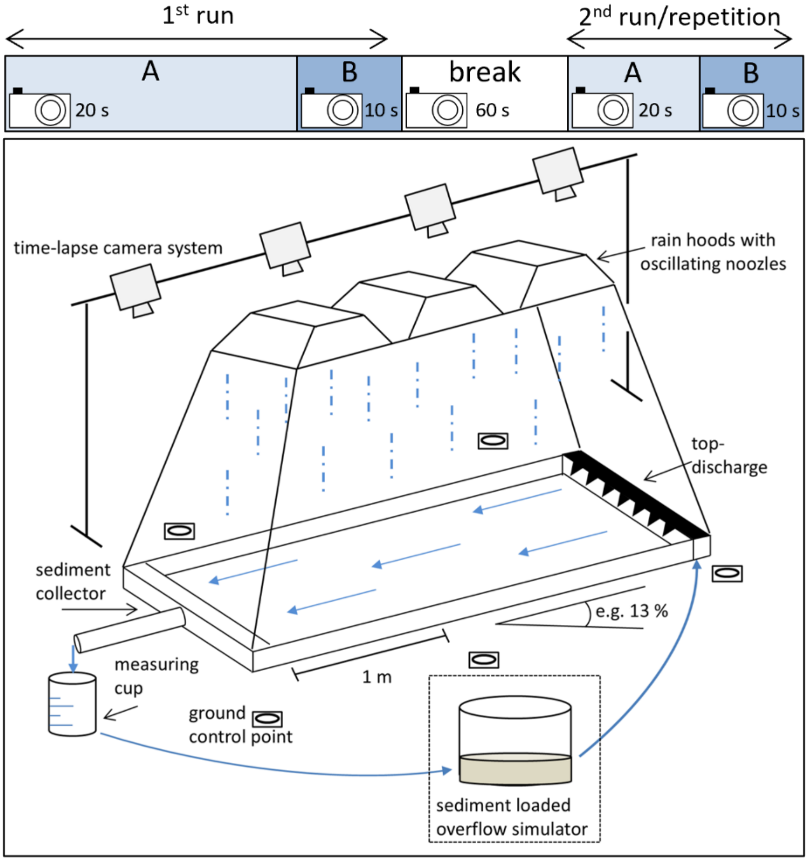

Figure 5: Schematic representation of an artificial rainfall simulation, as adapted from Schindewolf (2012) and monitored by a synchronised time-lapse camera system. The blue boxes at the top show the timeline of a rainfall simulation (1st run and 2nd run/repetition). Each run consists of an infiltration experiment (A) and a runoff experiment (B), separated by one-hour interval of no rainfall. The cameras indicate the frequency of the SfM (structure from motion) image taking, between every 10-60 s.

Soil samples were collected in the immediate vicinity of the plot at three distinct time points: prior to the experiment/ before 1st run A (six core samples), during the experimental break (three core samples) and after the end of the experiment/after 2nd run B (three core samples). The core samples were weighed in the laboratory both before and after drying, thus providing data on the bulk density and soil moisture content of the topsoil. The restricted spatial distribution and limited number of samples were a consequence of the lack of available space. Particle size distribution data were obtained using *ultrasonic dispersion* and *Köhn sieve sedimentation* techniques, applied to a subset of soil samples. The total organic carbon (TOC) was analysed using an elemental analyser coupled with *isotope ratio mass spectrometry (EA-IRMS*). The extent of surface vegetation and stones was estimated as a percentage, and the slope was measured. Figure 3 presents a summary of the data pertaining to soil, surface, rainfall and tillage conditions within the blue dashed box.

3 Data processing and results

Figure 6 shows the complete data processing workflow. Prior to data collection, all cameras used in terrestrial applications at the single slope and plots were pre-calibrated using a temporary calibration field (e.g., Eltner & James, 2022). The coordinates of the markers were determined with a mm-precision using a folding rule. The objective of the camera calibration was to ensure the precise modelling of the ray path from the object point through the camera's projection centre to the image sensor.

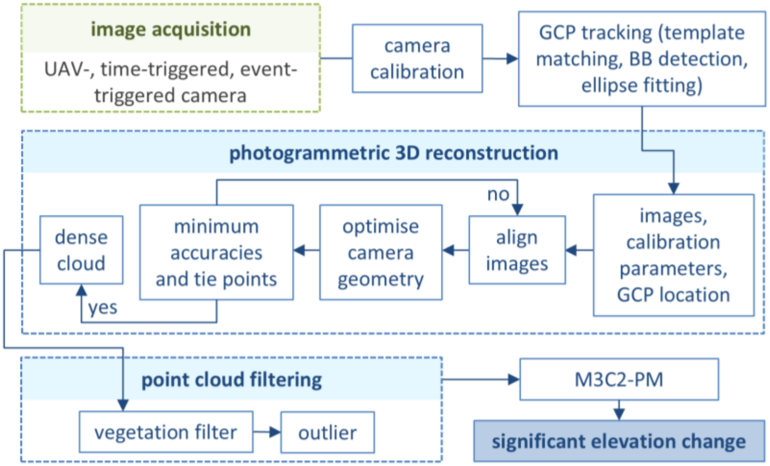

Figure 6: Image processing workflow adapted after Epple et al. (2025) (GCP = ground control point, M3C2 PM= Multiscale Model to Model Cloud Comparison with Precision Maps, BB detection = bounding box detection).

All cameras were synchronised during data capture using a wired connection between the cameras, thereby enabling simultaneous triggering. A~~While images a~~t the plot scale image match~~ed~~ing went well during the experiments lasting between 30 to 120 minutes.~~,~~ Due to the occurrence of clock drifts and trigger failures in the cameras over the four-year measurement period ~~Regarding at~~ at the field scale, an automatic time-matching approach was developed (Grothum et al., 2025)~~ due to the occurrence of clock drifts and trigger failures in the cameras over the four-year measurement period~~. In order to orient the image measurements and the resulting 3D models in a scaled reference frame, GCPs were utilised at the plot, slope and catchment setups. A *Leica TCRM 1102* total station, which can measur~~in~~e~~g~~ points with mm accuracy, was applied to map the GCP coordinates at the single slope and catchment. During the rainfall simulation, the GCPs were either measured by the same total station or using a ~~ruling~~ tape measure between the GCPs in combination with photogrammetric adjustment (as done in Eltner et al., 2017) to ~~also~~ get mm-accurate coordinates. The GCPs were automatically mapped in the images using a template matching approach based on normalized cross-correlation at the plots. At the field scale, a deep learning-based approach for bounding box detection was used, which demonstrated greater robustness throughout the year (Blanch et al., 2025). At the field scale, the coordinates of the GCPs were refined to sub-pixel accuracy through the application of ellipse-fitting (Grothum et al., 2025). A more detailed description of the technical procedure can be found in Grothum et al. (2025).

The external (camera poses, i.e., orientations and positions) and internal (only focal length and principle point) camera geometry were estimated within a bundle adjustment (using *Agisoft Metashape, v 1.8.3*) considering the pre-calibrated camera parameters, the GCPs and the tie points found via image matching. Furthermore, the precision of the tie points was estimated ~~using~~ by the M3C2-PM (multiscale model to model cloud comparison with precision maps) method (James et al., 2017). The adjustment was performed in an iterative manner, changing input parameters, such as number of required image point matches, if the overall accuracy was not sufficient. After image alignment and adjustment, a multi-view stereo (MVS) matching process was used to calculate the dense point clouds. Subsequently, the dense point clouds were subjected to filtering in order to remove any outliers and vegetation that may have been present (Grothum et al., 2023).

The point precisions of tie points were interpolated to the dense point cloud, thus enabling the subsequent derivation of a spatially distributed level of detection during change detection, i.e., point cloud differencing with the M3C2 approach (Lague et al., 2013). Each time series point cloud was compared with the initial point cloud in the series. A more detailed account of the whole data processing can be found in Grothum et al. (2025).

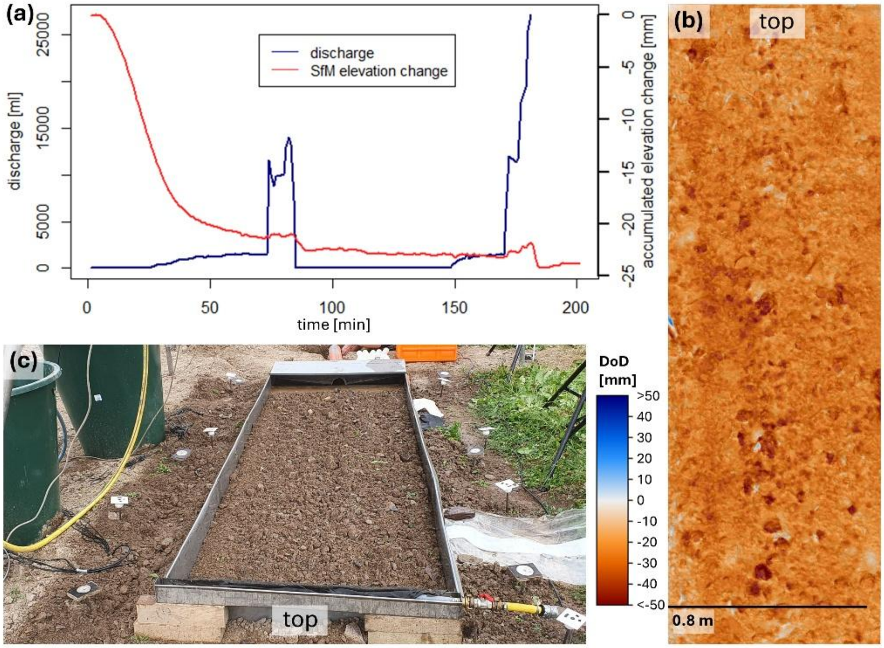

Figure 7: Rainfall simulation results on 2021-07-21 on the plot scale. (a) Timeline of the accumulated spatial averaged elevation change measured via SfM (structure from motion) and the measured discharge at the plot's outlet covering the whole simulation time. (b) DoD (digital elevation model of difference) subtracting dense 4 and dense 438 (captured before and after the rainfall simulation) presenting the spatially distributed elevation change. (c) Image of the rainfall simulation plot, shortly after the start.

Figure 7 presents the evaluation of data collected during the rainfall simulation 2021-07-21. The soil had been freshly cultivated~~grubbed~~ just two days prior, resulting in a loose and unconsolidated topsoil. As a result, a pronounced elevation decrease was observed at the beginning of the event (Fig. 7a), reflecting a combination of erosional and predominantly non-erosional processes such as compaction and consolidation. Epple et al. (2025), consider ten rainfall simulations of this dataset and provide on that base a detailed discussion of these initial elevation changes under varying soil conditions. ~~They~~ In this context they introduce an empirical method to distinguish non-erosional from erosional processes. The DEM of Difference (DoD) illustrates widespread surface lowering across the plot, with localized elevation losses exceeding 5 cm. These pronounced changes are attributed primarily to aggregate breakdown and other highly localized processes.

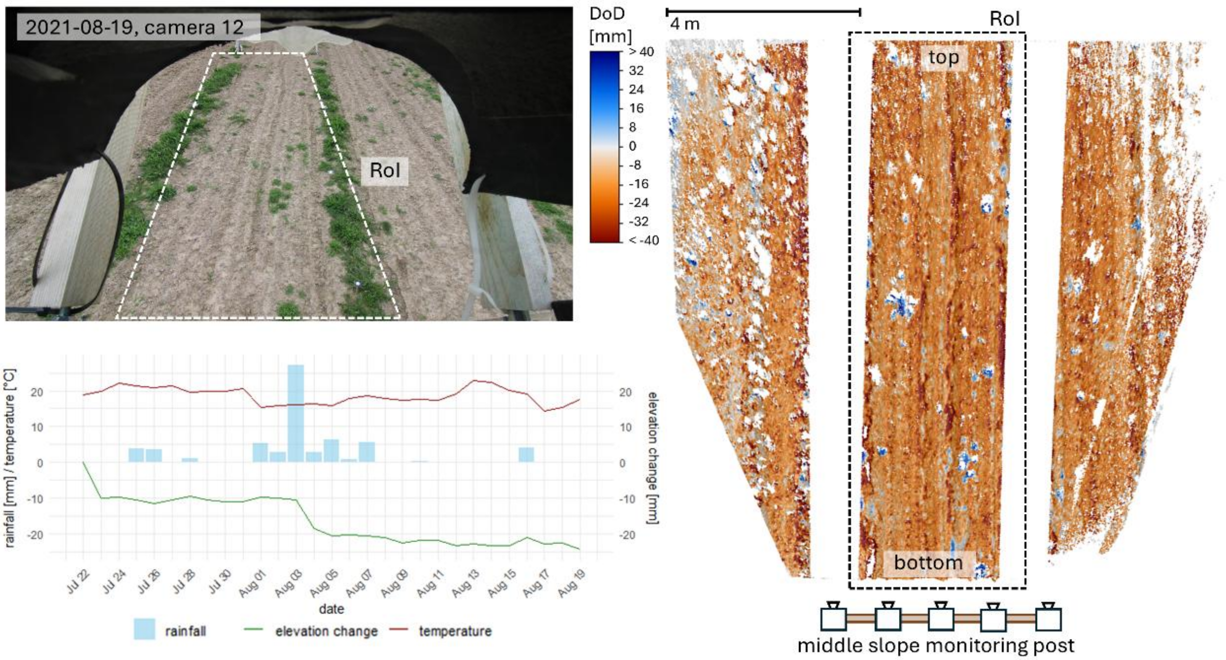

Figure 8: Results of a 28-days observation time at the middle slope position in July and August 2021. At the top: image of the camera 12, taken on 2021-08-19 at 10 ~~-~~a.m~~. CET.~~ At the bottom: timeline for the period 2021-07-22 (right after tillage) until 2021-08-19 (day before tillage), with the average M3C2 elevation change, the temperature and the daily rainfall. To the right: DoD (digital elevation model of difference) subtracting the days 2021-07-22 and 2021-08-19, with the schematic illustration of the middle slope monitoring post (bottom), cameras facing upslope. The RoI (region of interest) is marked by the dotted black/white box.

Figure 8 shows e~~E~~xemplary results on the slope scale~~ are presented in Fig. 8~~, visualising the changes in elevation~~ changes~~ during a 28-day observation period on the middle slope position in July and August 2021. Strongest elevation decreases were measured right after tillage ~~at~~on July 23rd and as a result of heavy rainfall on August 3rd (Fig. ~~-~~8, timeline). The DoD illustrates strongest elevation decreases along the tillage lines, the predominant flow paths, which lead to~~ …~~ rill erosion. Elevation increases (blue patterns in the DoD) are a result of vegetation growth, as can be seen in the image at the top.

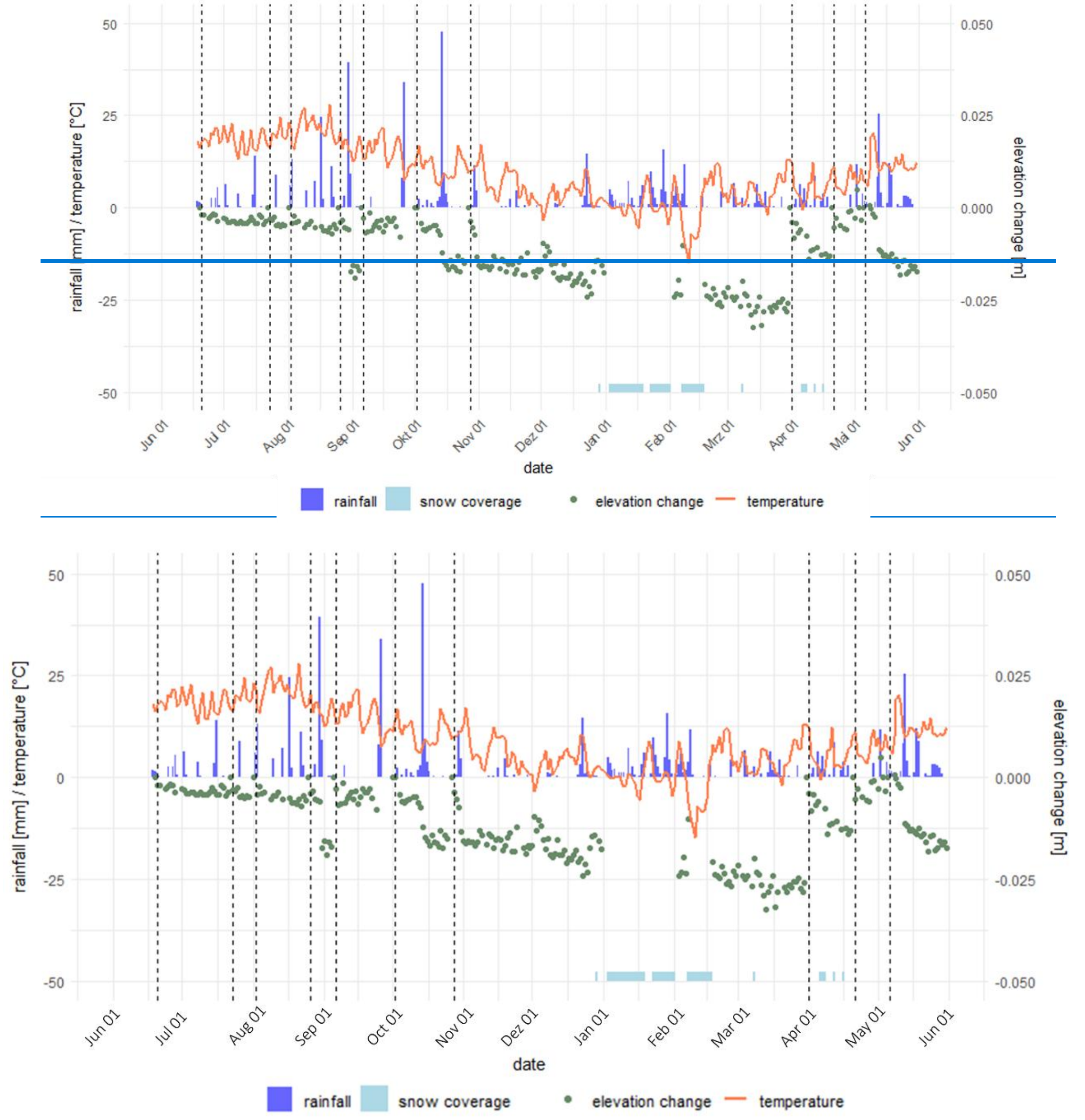

Figure 9: Timeline presenting the averaged M3C2 elevation change development over the year June 2020 until June 2021 measured by the middle slope monitoring post (dotted vertical lines indicate tillage and therefore an elevation reset).

~~Next~~ In addition to the information on single rainfall simulations and a month of rainfall events, the data offer information on a yearly scale. Figure ~~-~~9 presents 12 months of elevation change in 2020-2021 recorded at the middle slope position. With no tillage and therefore no reset from Novembre 2020 until April 2021, information about the seasonal development during the winter months can be derived. Small rainfall events, snow coverage and snow melting lead to an average decrease of 3 cm during these months. As already presented in Fig. 7 the data show ~~the~~ high potential for consolidation and compaction on the site right after tillage. At this time, already small rainfall events can lead to comparable high elevation decreases (e.g., O~~k~~ctober 2020).

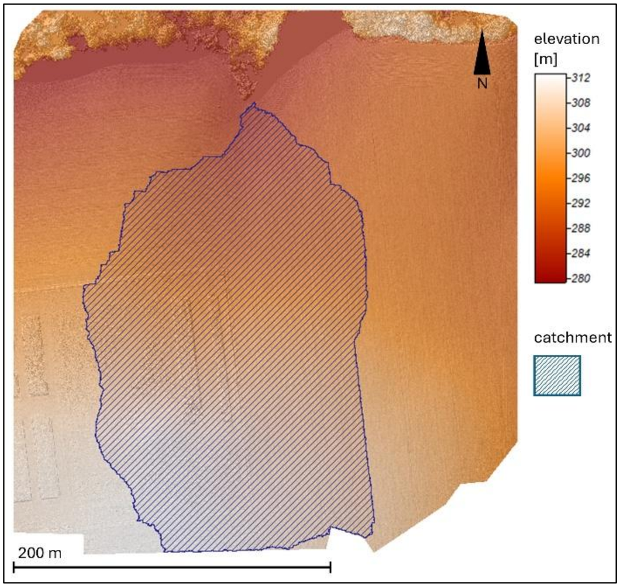

Figure 10: DEM (digital elevation model) of the catchment scale (2020-07-22), with the catchment marked in blue, visualised with an analytic hillshade in the back.

Figure 10 presents the information, available on the catchment scale. Both the slope as well as ten of the plot positions are nested within this blue area. This dataset as well as the UAV-images of eight further flights~~days~~ during the monitoring period are an important part of this nested experimental setup. It serves on the one hand as model input for soil erosion modelling at the catchment scale and provides on the other hand a data base for upscaling approaches~~.~~, ~~This~~ offering~~s~~ processed-based soil erosion modelling, the opportunity to test the plot-calibrated and slope-validated information on the ~~catchment scale~~next scale.~~This dataset as well as the UAV-images of eight further days during the monitoring period are an important part of this nested experimental setup~~

4 Structure of the data archive

The dataset is structured according to the three scales: plot, slope and catchment (Fig. 11). Each observation scale is divided into two datasets: a raw and a processed one. The raw dataset comprises the unprocessed images (from the terrestrial used SLR and the UAV cameras), 3D coordinates of the GCPs (i.e., in object space) and empirical field data (rainfall simulation results, soil data, meteorological data, etc.). The processed data set includes the camera calibration protocols, the reconstructed dense point clouds, the orthophotos, the point precision maps and the M3C2 distances per point. Please find a detailed overview of the data in the data description accompanying the data.

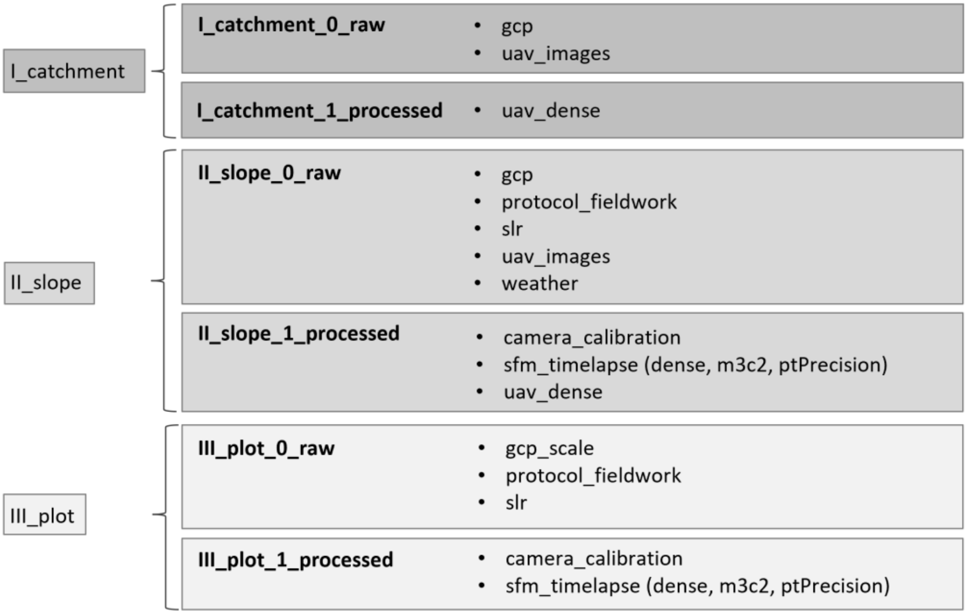

Figure 11: Dataset structured by the observation scales and further subdivided into raw and processed data. (gcp = ground control point, slr = single lens reflex, uav = uncrewed aerial vehicle, sfm = structure from motion, ptPrecision = point precision map; lowercases used as in the data archive)

5 Data quality

Table 2: Average accuracy metrics of the plot and slope data, excluding strong outliers. CP and GCP refer to check point and ground control point respectively, std dev stands for standard deviation.

	plot	slope
average median error [mm]	2.7	5.0
average std dev error [mm]	2.8	4.9
median CP error [mm]	2.5	6.1
std dev error CP [mm]	4.3	10.8
median GCP error [mm]	1.8	1.2
std dev error GCP [mm]	2.5	1.7

An overview of the accuracies can be found in Tab. 2. The point precision files (ptPrecision) in the ‘time~~-~~lapse’ folders within the dataset offer mm-precisions on every connection point in every 3D-model on both plot and slope scale, averaged by the ~~“~~‘average median error~~”~~’~~ (Tab. 2)~~. Information on the RMSE (root mean square error) at the GCPs and CPs for every

3D-model are included as log-files in the ‘time_lapse’ folder. ~~The median and standard deviation (std dev) is summarised in Tab. 12, respectively.~~

6 Data availability

The described data set can be found by the following DOI:
Final DOI will be added with the acceptance of the manuscript. In this way, the data can still be adapted according to the reviewers' comments – proposed way by ESSD. With the final upload the data will be stored in folders named plot, slope, catchment and make available via DOI. The data will be shared via https://opara.zih.tu-dresden.de/home.

7 Code availability

The code for photogrammetric time-lapse data processing has been published by Grothum et al. (2025).

8 Recommendations and conclusions

We introduce a novel ~~and unprecedented~~ nested dataset designed for the detection and analysis of soil surface changes, which we make available to the broader scientific community. This dataset provides high-resolution spatio-temporal data on geomorphological processes, including erosion triggered by heavy rainfall and seasonal elevation changes. It spans a range of spatial scales, from 3 m² to 5 ha, and includes variable data acquisition frequencies, offering a distinctive resource for in-depth examination of soil dynamics. To ensure maximal transparency, we provide both the raw data required to construct DEMs and pre-processed dense point clouds for further use. While the current dataset is based on a loess site in eastern Germany with a limited slope range and moderate rainfall events, we encourage researchers to expand its scope. This can be achieved by integrating camera systems during rainfall simulations and collecting high-resolution spatial and temporal data during natural rainfall events. For this purpose, both software and hardware are made openly accessible and adaptable to other locations and conditions. Such contributions will enable to address existing challenges in soil erosion modelling by providing new observations for model evaluation and calibration. Furthermore, this unique dataset offers a first-of-its-kind opportunity to train artificial intelligence (AI) models and compare their performance with conventional process-based soil erosion models. We anticipate that this dataset will significantly enhance the understanding of soil erosion processes and contribute to the development of more accurate and robust predictive models.

Acknowledgements

We would like to thank the Research Group (Flow and Transport Modeling in the Geosphere) of the TU Bergakademie Freiberg for their support with the rainfall simulations and their laboratory analyses, the TLLLR (Thuringian State Office for Agriculture and Rural Areas) for the provision of agricultural land in Thuringia for rainfall simulations, and the LfULG (Saxon State Office for Environment, Agriculture and Geology, Germany) for the provision and management of agricultural land over the past four years. We would like to thank the editor and reviewers for their insightful comments, which have greatly improved the quality and clarity of our manuscript. We sincerely appreciate their time and effort in reviewing our paper.

Funding

The work was supported by the German Research Foundation (Deutsche Forschungsgemeinschaft, DFG 405774238) in the project “High resolution photogrammetric methods for nested parameterisation and validation of a physical based soil erosion model”.

9 References

Batista, P. V., Davies, J., Silva, M. L., and Quinton, J. N.: On the evaluation of soil erosion models: Are we doing enough?, Earth-Sci. Rev., 197, 102898, https://doi.org/10.1016/j.earscirev.2019.102898, 2019.

Blanch, X., Guinau, M., Eltner, A., and Abellan, A.: A cost-effective image-based system for 3D geomorphic monitoring: An application to rockfalls, Geomorphology, 449, 109065, https://doi.org/10.1016/j.geomorph.2024.109065, 2024.

~~Blanch, X., Eltner, A., Guinau, M., and Abellan, A.: Multi-Epoch and Multi-Imagery (MEMI) Photogrammetric Workflow for Enhanced Change Detection Using Time-Lapse Cameras, Remote Sens., 13, 1460, https://doi.org/10.3390/rs13081460, 2021.~~

Blanch, X., Jäschke, A., Elias, M., and Eltner, A.: Subpixel Automatic Detection of GCP Coordinates in Time-Lapse Images Using a Deep Learning Keypoint Network, IEEE Trans. Geosci. Remote Sens., 63, 1-14, https://doi.org/10.1109/TGRS.2024.3514854, 2025.

Ehrhardt, A., Deumlich, D., and Gerke, H. H.: Soil Surface Micro-Topography by Structure-from-Motion Photogrammetry for Monitoring Density and Erosion Dynamics, Front. Environ. Sci., 9, https://doi.org/10.3389/fenvs.2021.737702, 2022.

Eltner, A., Baumgart, P., Maas, H.-G., and Faust, D.: Multi-temporal UAV data for automatic measurement of rill and interrill erosion on loess soil. Earth Surf. Proc. and Land., 40, 6, 741-755, 2015.

Eltner, A., Kaiser, A., Abellan, A., and Schindewolf, M.: Time lapse structure-from-motion photogrammetry for continuous geomorphic monitoring, Earth Surf. Proc. Land., 42, 2240-2253, https://doi.org/10.1002/esp.4178, 2017.

Eltner, A. and Sofia, G.: Structure from motion photogrammetric technique, Remote Sensing of Geomorphology, Elsevier, 1-24, https://doi.org/10.1016/B978-0-444-64177-9.00001-1, 2020.

Eltner, A. and~~,~~ James, M.: Guidelines for flight operations. 75-86. In: Eltner, A., Karrasch, P., Stöcker, C., Klingbeil, L., Hoffmeister, D., Kaiser, A., Rovere, A. (editors): UAVs in Environmental Sciences – Methods and Applications. WBG Academic, 492 pp., ISBN 9783534405886, 2022.

Eltner, A., Favis-Mortlock, D., Grothum, O., Neumann, M., Laburda, T., and Kavka, P.: Using 3D observations with high spatio-temporal resolution to calibrate and evaluate a process-focused cellular automaton model of soil erosion by water SOIL, 11, 413–434, https://doi.org/10.5194/soil-11-413-2025, 2025.

Epple, L., Grothum, O., Bienert, A., and Eltner, A.: Decoding rainfall effects on soil surface changes: Empirical separation of sediment yield in time-lapse SfM photogrammetry measurements, Soil and Till. Res., 248, 106384, https://doi.org/10.1016/j.still.2024.106384, 2025.

Epple, L., Kaiser, A., Schindewolf, M., Bienert, A., Lenz, J., and Eltner, A.: A Review on the Possibilities and Challenges of Today's Soil and Soil Surface Assessment Techniques in the Context of Process-Based Soil Erosion Models, Remote Sens., 14, 2468, https://doi.org/10.3390/rs14102468, 2022.

Favis-Mortlock, D.: github.com/davefavismortlock/RillGrow [last accessed: 19.06.2025], 2025.

Grothum, O., Bienert, A., Blümlein, M., and Eltner, A,: Using machine learning techniques to filter vegetation in colorized SfM point clouds of soil surfaces. Int. Arch. Photogramm. Remote Sens. Spatial Inf. Sci., XLVIII-1/W2-2023, 163-170, https://doi.org/10.5194/isprs-archives-XLVIII-1-W2-2023-163-2023, 2023.

Grothum, O., Epple, L., Bienert, A., Blanch, X., and Eltner, A.: Near-continuous observation of soil surface changes at single slopes with high spatial resolution via an automated SfM photogrammetric mapping approach, EGUsphere [preprint], https://doi.org/10.5194/egusphere-2025-2291, 2025.

Hänsel, P., Schindewolf, M., Eltner, A., Kaiser, A., and Schmidt, J.: Feasibility of High-Resolution Soil Erosion Measurements by Means of Rainfall Simulations and SfM Photogrammetry, Hydrol., 3, 38, https://doi.org/10.3390/hydrology3040038, 2016.

James, M. R., Robson, S., and Smith, M. W.: 3-D uncertainty-based topographic change detection with structure-from-motion photogrammetry: precision maps for ground control and directly georeferenced surveys, Earth Surf. Process. Land., 42, 1769–1788, https://doi.org/10.1002/esp.4125, 2017.

Jetten, V. and Favis-Mortlock, D.: Modelling Soil Erosion in Europe, in: Soil Erosion in Europe, edited by: Boardman, J. and Poesen, J., John Wiley & Sons, Ltd, Chichester, UK, 695–716, https://doi.org/10.1002/0470859202.ch50, 2006.

Jiang, Y., Shi, H., Wen, Z., Guo, M., Zhao, J., Cao, X., Fan, Y., and Zheng, C.: The dynamic process of slope rill erosion analyzed with a digital close range photogrammetry observation system under laboratory conditions, Geomor., 350, 106893, https://doi.org/10.1016/j.geomorph.2019.106893, 2020.

Kainz, M., Auerswald, K., and Vöhringer, R.,: Comparison of german and swiss rainfall simulators – utility, labour demands and costs. Z. Pflanzenernahr. Bodenkd. 155, 1, pp. 7-11, 1992.

Lague, D., Brodu, N., and Leroux, J.: Accurate 3D comparison of complex topography with terrestrial laser scanner: Application to the Rangitikei canyon (N-Z), ISPRS J. of Photogramm. and Remote Sens., 82, 10–26, https://doi.org/10.1016/j.isprsjprs.2013.04.009, 2013.

Naranjo, S., Rodrigues Jr., F. A., Cadisch, G., Lopez-Ridaura, S., Fuentes Ponce, M., and Marohn, C.: Effects of spatial resolution of terrain models on modelled discharge and soil loss in Oaxaca, Mexico, Hydrol. Earth Syst. Sci., 25, 5561-5588, https://doi.org/10.5194/hess-25-5561-2021, 2021.

Pandey, A., Himanshu, S. K., Mishra, S. K., and Singh, V. P.: Physically based soil erosion and sediment yield models revisited, CATENA, 147, 595-620, https://doi.org/10.1016/j.catena.2016.08.002, 2016.

Schindewolf, M.: Prozessbasierte Modellierung von Erosion, Deposition und partikelgebundenem Nähr- und Schadstofftransport in der Einzugsgebiets- und Regionalskala, Dissertation, TU Bergakademie Freiberg, Freiberg, 2012.

Schindewolf, M. and Schmidt, J.: Parameterization of the EROSION 2D/3D soil erosion model using a small-scale rainfall simulator and upstream runoff simulation, CATENA, 91, 47-55, https://doi.org/10.1016/j.catena.2011.01.007, 2012.

~~Wang, H., Pang, G., Yang, Q., Long, Y., Wang, L., Wang, C., Hu, S., Wang, Z., and Yang, A.: Effects of slope shape on soil erosion and deposition patterns based on SfM-UAV photogrammetry, Geoderma, 451, 117076, https://doi.org/10.1016/j.geoderma.2024.117076, 2024.~~

Yang, Y., Shi, Y., Liang, X., Huang, T., Fu, S., and Liu, B.: Evaluation of structure from motion (SfM) photogrammetry on the measurement of rill and interrill erosion in a typical loess, Geomor., 385, 107734, https://doi.org/10.1016/j.geomorph.2021.107734, 2021.